Characterization of a Temperature-Controlled FAIMS System

David A. Barnett, Michael Belford, Jean-Jacques Dunyach, and Randy W. Purves*

Thermo Fisher Scientific, San Jose, California, USA

High-field asymmetric waveform ion mobility spectrometry (FAIMS) focuses and separates gas-phase analyte ions from chemical background, offering substantial improvements in the detection of targeted species in biological matrices. Ion separations have been typically performed at atmospheric pressure and ambient temperature, although routine small molecule quantitation by LC-MS (and thus LC-FAIMS-MS) is generally performed at liquid flow rates (e.g., in excess of 200 μL/min) in which atmospheric pressure ionization sources (e.g., APCI and ESI) need to be run at elevated temperatures to enhance ion desolvation. Heat from the ionization source and/or the mass spectrometer capillary interface is shown to have a significant impact on the performance of a conventional FAIMS electrode set. This study introduces a new FAIMS system that uses gas heating/cooling to quickly reach temperature equilibrium independent of the external temperature conditions. A series of equations and balance plots, which look at the effect of temperature and other variables, on the normalized field strength (E/N), are introduced and used to explain experimental observations. Examples where the ion behavior deviates from the predicted behavior are presented and explanations based on clusters or changes in ion-neutral interactions are given. Consequences of the use of temperature control, and in particular advantages of using different temperature settings on the inner and outer electrodes, for the purpose of manipulating ion separation are described.   (J Am Soc Mass Spectrom 2007, 18, 1653–1663) © 2007 American Society for Mass Spectrometry

B ecause of its high sensitivity and selectivity, liquid chromatography combined with tandem mass spectrometry (LC-MS/MS) has become the method of choice for quantitation of bioorganic compounds in biological matrices such as urine or blood plasma [1–3]. To preserve LC conditions and flow rates typically used with LC-UV (e.g., 1 mL/min), mass spectrometer manufacturers needed to adapt electrospray ionization (ESI) sources, which were initially operated at much lower liquid flow rates [4, 5], to achieve sufficient ion desolvation. Consequently, sources that use the addition of heat to accelerate ion desolvation were created [6, 7] and further developed into the commercial sources that are used today (e.g., Heated Electrospray; H-ESI™ and TurboIonSpray; TIS™). Despite the widespread utility offered by LC-MS/MS, because of the complexity of biological matrices, in many instances (e.g., high background [8], co-eluting interferences [9]) additional selectivity in an analysis is still required.

High-field asymmetric waveform ion mobility spectrometry (FAIMS) is a gas-phase ion-separation technique that is based on compound-dependent differences in an ion's mobility at high field (K_h) relative to low field (K) [10, 11]. With FAIMS, deviations in ion mobility resulting from the high electric fields are reflected experimentally by the compensation voltage (CV) of transmission for a particular analyte. Consequently, by fixing the CV value, a subset of ions is allowed to pass through the FAIMS, whereas other ions are lost to the walls of the device. FAIMS is readily coupled between an atmospheric pressure ionization source and a mass spectrometer [12–16] and, because of its unique ion-separation mechanism [17], FAIMS offers additional selectivity for bioanalytical applications. Indeed, FAIMS has been previously interfaced to atmospheric pressure ionization sources such as ESI [12] and APCI [8] operating at low liquid flow rates (and thus low temperatures) and has been found to significantly lower detection limits by reducing background ion current without sacrificing absolute signal intensity [18–20]. Although FAIMS is readily interfaced to heated ionization sources capable of operating at higher liquid flow rates, heat from these sources will have a significant impact on the performance of the FAIMS electrodes as will be subsequently described in more detail.

The passive heating of the FAIMS electrode set from a heated ionization source requires approximately 2 h of equilibration time for stable operating conditions to

Address reprint requests to Dr. Randall W. Purves at Merck Frosst Canada Ltd., 16711 Trans Canada Highway, Montreal, Quebec, Canada H9H 3L1. E-mail: randall_purves@merck.com

* Present address: Merck Frosst Canada Ltd., 16711 Trans Canada Highway, Kirkland, QC, Canada H9H 3L1.

be reached [21] and this amount of equilibration time is clearly unacceptable for routine analysis. Furthermore, changes in the FAIMS electrode temperature will also affect how the ions are separated. In addition, any other heat sources that may be present in the source region will also affect the temperature of the FAIMS electrodes (e.g., the heated ion transfer capillary on the TSQ Quantum Ultra mass spectrometer). Consequently, eliminating the effect of heat from ionization, or any heat source, on the temperature of the FAIMS electrodes is a necessary evolution of the FAIMS device for improving its performance. Fast initial FAIMS electrode temperature stabilization and the need for the FAIMS electrode temperature to adjust quickly to changes in source/interface temperature are required.

A new temperature-controlled FAIMS electrode is examined in this study. The role of temperature in ion separation within a FAIMS device is explored. Equations that dictate how temperature will affect FAIMS performance are subsequently reviewed and examples are given that illustrate their effect. Deviations from predicted ion behavior are presented and the role of clusters and ion-neutral interactions with changes in temperature are discussed.

Background: Effect of Temperature on Electric Fields within FAIMS

The effect of temperature on the ion behavior in a FAIMS device can be described, to a large extent, from the ion mobility equations found in the literature. This section is designed to review concepts that will be necessary for discussing the effect of temperature on the fields, and thus ion separation, within FAIMS. Because the FAIMS is operating at or near atmospheric pressure, the velocity v_d (cm/s) of an ion in a bath gas under the influence of an electric field E (V/cm) can be described as follows [22]:

$$v_d = K(E/N) \tag{1}$$

where K is the ion mobility constant (typically reported in units of $cm^2\ s^{-1}\ V^{-1}$) and N is the gas number density (cm^{-3}). At low fields (low E/N magnitude), the value of K is independent of E/N. As the field strength is increased, eventually the value of K will begin to change. Experimentally, the value of E (at atmospheric pressure and room temperature) required for changes in K to occur has been found to be as low as 2500 V/cm [23]; however, this value is ion dependent. The mobility at higher E/N (K_h) for a given ion can be expressed as

$$K_h(E/N) = K[1 + f(E/N)] \tag{2}$$

Experimentally, the ratio of K_h/K can be derived from a series of CV/DV plots [17]; CV/DV plots are described in more detail in Results and Discussion. The value of N in the preceding equations can be calculated as follows:

$$N = (n/V) * N_A \tag{3}$$

where N_A is Avogadro's constant ($6.022 \times 10^{23}\ mol^{-1}$) and (n/V) can be calculated from the ideal gas law:

$$(n/V) = p/RT \tag{4}$$

Here R is $0.8206\ L\ atm^{-1}\ mol^{-1}\ K^{-1}$; p (atm) and T (K) are parameters that are measured during the experiment. To calculate the electric fields in the cylindrical FAIMS device used in this study, consider Figure 1. Figure 1a shows a three-dimensional schematic of the temperature-controlled FAIMS device used in this study (described in more detail in the experimental section) and Figure 1b is obtained by taking a cross section of the device. As was described previously [17], when a voltage is applied to the inner cylinder, the voltage V(r), at any radial location between the two cylinders, can be calculated as:

$$V(r) = Va[\ln(r/b)/\ln(a/b)] \tag{5}$$

where Va is the potential applied to the inner cylinder, "a" represents the outer radius of the inner cylinder, and "b" represents the inner radius of the outer cylinder as is shown in the figure.

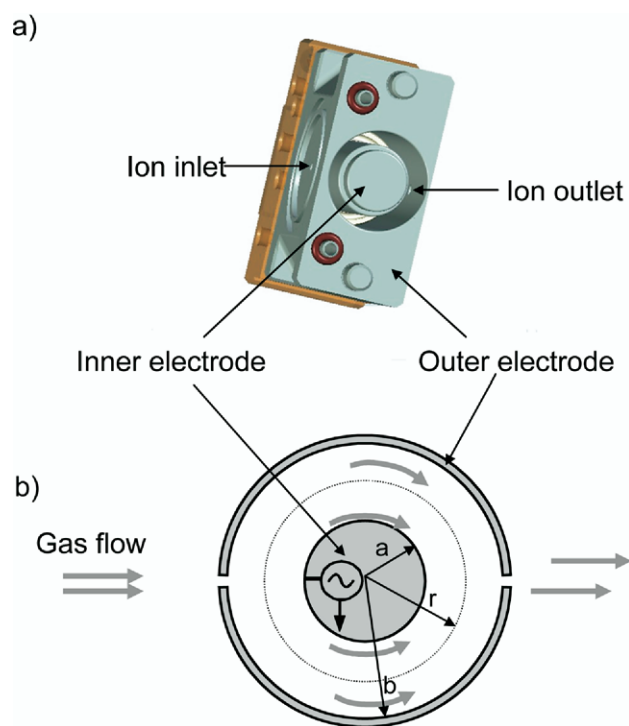Because the voltage does not vary in a linear fashion between the cylinders, the electric field is nonuniform

Figure 1. (a) Three-dimensional schematic of a temperature controlled FAIMS device, (b) cross section of the FAIMS device illustrating radial location, r, between the walls of the inner electrode, "a" and outer electrode "b." The asymmetric waveform is applied to the inner electrode.

between the two cylinders and at any point r can be shown to be

$$E_r = -Va/[r \ln(a/b)] \qquad (6)$$

This nonuniform electric field between the two cylinders is essential for atmospheric pressure ion focusing as described previously [17]. For illustrative purposes, the electric field for a flat plate FAIMS device (E_{flat}) will also be introduced, where

$$E_{flat} = -Va/(b - a) \qquad (7)$$

Experimental

A schematic of the FAIMS electrode design used in this study is shown in Figure 1a. The electrode design consists of two concentric stainless steel cylinders mounted inside poly(ether ether ketone) (PEEK) housing and attached to the atmospheric pressure ionization interface of a TSQ quantum Ultra triple-quadrupole mass spectrometer (Thermo Fisher Scientific, San Jose, CA). The cylindrical electrodes are mounted perpendicular to the source and MS orifice with the FAIMS ion inlet and outlet on the same plane as the inlet to the mass spectrometer. A waveform generator was used to apply the asymmetric waveform (the maximum value of the asymmetric waveform is referred to as dispersion voltage or DV), and compensation voltage (CV; i.e., dc voltage difference between the inner and outer cylinders). The asymmetric waveform was composed of a 2:1 ratio of a 750-kHz sinusoidal wave and its first harmonic [24]; the maximum voltage (i.e., DV) was ±5300 V. A constant dc bias of ±35 V was applied to the outer cylinder (9.0-mm inner radius) of the FAIMS device and to the inlet of the mass spectrometer. Three different inner electrodes were manufactured for use with the FAIMS device in this study. The majority of the data were acquired using an inner electrode having an outer radius of 6.5 mm (2.5-mm gap between the inner and outer electrode). For studies involving changing FAIMS geometries, two additional inner electrodes were also used having outer radii of 6.0 mm (3.0-mm gap) and 7.0 mm (2.0-mm gap).

The heated electrospray ionization (H-ESI) source was operated at +4000 V (positive mode) or −3000 V (negative mode). The sheath and auxiliary gases were set to "40" and the temperature of the vaporizer was varied depending on the sample (given in text). Ions from the H-ESI source passed through the entrance plate (2.5-mm orifice) and entered the FAIMS device through a 1.5-mm aperture in the outer electrode. Variable flows of high-purity nitrogen gas (MEGS, Ottawa, Ontario, Canada) and industrial helium gas (BOC, Ottawa, Ontario, Canada) were passed through separate charcoal/molecular sieve filters, combined in a tee assembly, and introduced into the gap (~1.5 mm) between the entrance plate and the outer electrode. The combined gas flow rate was 2.5 L/min for a sample

flow rate of 50 μL/min and 4 L/min for a sample flow rate of 400 μL/min. The majority of this gas exited through the entrance plate countercurrent to the ESI-generated ions, aiding in their desolvation. The remainder of the gas was drawn into the FAIMS analyzer at the same flow rate (~1.2 L/min) as the gas intake of the mass spectrometer (because the electrode is gastight on the surface of the ion inlet of the mass spectrometer), carrying the ions around both sides of the inner cylindrical electrode and in through the inlet capillary (580 μm) of the mass spectrometer. Individual gas flows were adjusted using mass flow controllers (MKS Type 1179A; MKS Instruments, Andover, MA). Using appropriate combinations of DV and CV, ions could be selectively transmitted through FAIMS and sampled by the mass spectrometer.

To control the temperature of the electrode set, channels for the passage of heated gas were drilled into both electrodes. The intense RF field applied to the inner electrode prevented direct heating of this electrode with a resistive element. The outer electrode consists of a cylinder with i.d. of 18 mm bored into a solid block of stainless steel; channels to the left and right of the cylinder carry cool or heated air in and out of the block. The inner electrode has a PEEK insert that directs gas to the top of the electrode and then along the inner surface of the electrode to an exhaust port. The mass of the inner electrode is lower than that of the outer electrode. Care was taken to minimize the mass of both electrodes to achieve the fastest possible temperature response. A gas heater assembly containing two separate 200-Watt heater cartridges for the inner and outer electrode gas was mounted near the electrodes. Thermocouples were positioned in the heater gas exhaust lines as near as possible to the electrodes, thereby providing a feedback mechanism to adjust the power delivered to the heating cartridges. Using a gas for temperature control also offers an ability to cool the electrodes to room temperature. This cooling functionality could not be achieved with conventional heating elements. Under conditions of active heating of the electrodes, the inner electrode temperature is stable to within ±1 °C of the set point (35–120 °C) after 2 min of heating. Heating of the outer electrode requires more time to reach a stable value due to its larger mass; however, it too is stable to within ±1 °C after about 5 min.

Neat stock solutions of cesium iodide (10 mM), methotrexate (1 mg/mL), gramicidin S (1 mg/mL), lidocaine (1 mg/mL), and taurocholic acid (1 mg/mL) were prepared in distilled deionized water. Individual samples for analysis were prepared in 70/30 (vol/vol) methanol/water containing 0.1% formic acid at 10 ng/μL concentrations except for cesium iodide (1 mM). Sample solutions were infused by a Hamilton syringe pump at 2 μL/min and diluted in a tee union with either 48 or 398 μL/min of the methanol/water/formic acid mobile phase.

Results and Discussion

The Temperature Issue and Establishing Temperature Control

There are two sources of heat in the interface region of a TSQ Quantum Ultra triple quadrupole mass spectrometer: the heated electrospray ionization probe (H-ESI™) and the heated capillary inlet. Typical settings for the H-ESI probe and heated capillary are 350 and 300 °C, respectively, when using sample flow rates > 200 μL/min delivered directly to the source of the mass spectrometer. To illustrate the effect of heat on the performance of the FAIMS device, the gas flows that allow temperature control of the FAIMS were not activated. A solution containing cesium iodide was infused and CV spectra were acquired. Because the high-field mobility of the cesium cation in a carrier gas of nitrogen increases with increasing electric field strength (i.e., $K_h/K > 1$), application of a positive polarity asymmetric waveform and negative polarity compensation voltage was required for the transmission of the cesium cation through a cylindrical focusing FAIMS device [12]. The effect of heat on the FAIMS device is shown in Figure S1 (in the Supplementary Material section, which can be found in the electronic version of this article). The figure shows that when no external heat is applied to the FAIMS (i.e., vaporizer and capillary temperatures are set to 0 °C; actual values are near room temperature), the cesium ion is transmitted through FAIMS at a CV of −20.2 V (dashed trace). When the vaporizer temperature is set to 350 °C, and 2 h are allowed for temperature equilibration, a CV spectrum (solid trace) shows an increase in magnitude of the CV to −28.5 V and an accompanying increase in the width of the CV peak. The effect of raising the capillary temperature to 300 °C (while holding the vaporizer temperature at 0 °C) is similar but not as dramatic; the CV is increased from −20.2 V at room temperature ($T_{capillary}$ = 0 °C) to −22.6 V at 300 °C after 2 h (not shown). Note that to avoid ambiguity that may be caused by peak distortion near the peak maxima, or for peaks that are very wide, optimal CV values were calculated by determining the midpoint between the CV values on each side of the peak at 50% peak height. A sample calculation is illustrated in Figure S1 for the spectrum obtained with the vaporizer set to room temperature. The CV values at 50% of the maximum peak height are −18.4 and −22.0 V, resulting in a CV value of −20.2 V. These observed shifts in CV with interface temperatures and the lengthy temperature equilibration times (∼2 h) illustrate the need for a temperature-controlled FAIMS system.

Using active temperature control of the electrodes, the capability to control the electrode temperature independently of the ion source settings was examined. The independence of the electrode temperature from the ion source temperature setting is demonstrated using the cesium ion at three different electrode tem-
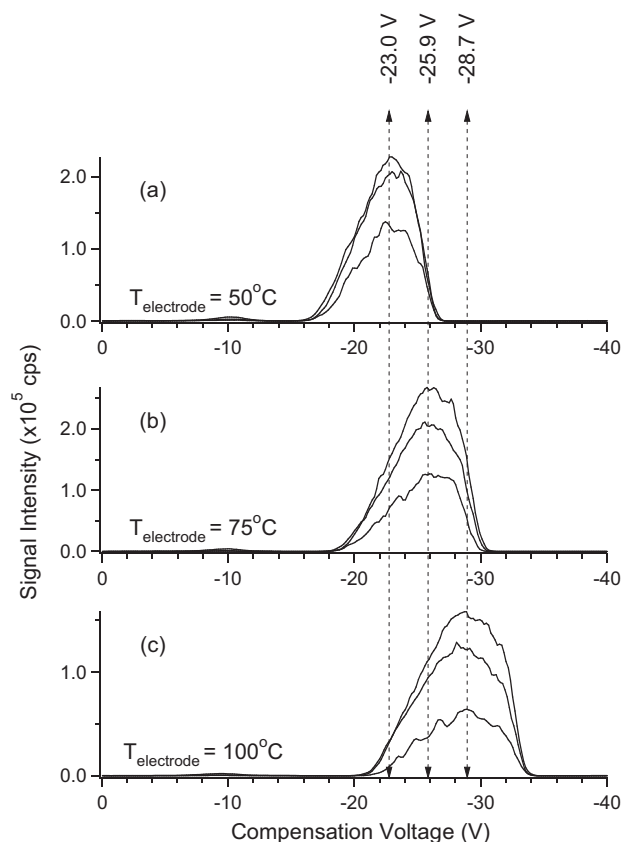

Figure 2. Stability of cesium ion transmission at electrode temperature set points of (**a**) 50 °C, (**b**) 75 °C, and (**c**) 100 °C when varying the vaporizer temperature between room temperature (i.e., 0 °C), 175 °C, and 350 °C.

perature set points (both electrodes were operated at the same value). Figure 2 shows CV plots that were obtained using three different vaporizer temperatures: room temperature (i.e., 0 °C), 175 °C, and 350 °C at each electrode set point; 50 °C (Figure 2a), 75 °C (Figure 2b), and 100 °C (Figure 2c). Although there are modest variations in signal strength, the plots for different vaporizer conditions at a given electrode temperature remain virtually identical in terms of the CV axis. Consequently, Figure 2 illustrates that the compensation voltage remains stable (implying that the temperature of the FAIMS is also held at a constant value) independent of the source conditions, a necessity for using FAIMS for bioanalyses.

The Use of CV/DV and CF/DF Plots

Plots of the CV as a function of the DV (i.e., CV/DV plots) have been used to illustrate ion focusing and describe peak shape within a FAIMS device [17, 25]. These plots (and CF/DF plots defined below) are critical for explaining the role of temperature in a FAIMS device. A brief review of the utility of this type of plot is subsequently described using Figure 3 as an illustration. Using active temperature control and setting the temperature of both electrodes to 36 °C, CV spectra for
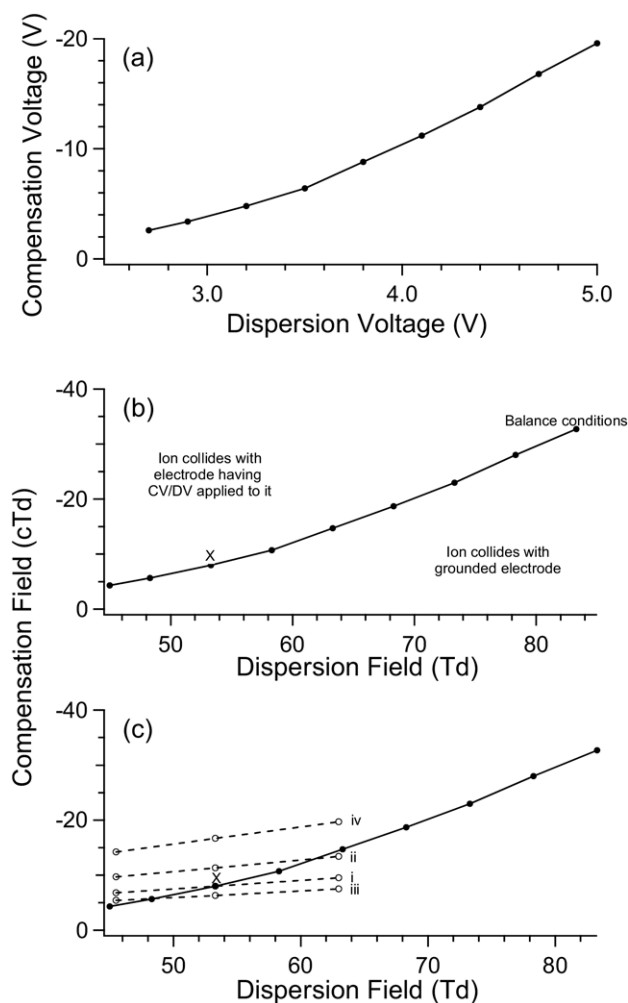
Figure 3. CV/DV and CF/DF plots. (**a**) CV/DV plot generated for the cesium ion by experimentally taking the optimum CV value of ion transmission for each DV value. (**b**) Conversion of the CV/DV plot to a CF/DF plot for a flat plate FAIMS device. In this device, an ion is only stable between the electrode walls if it remains on the balance line shown on the figure. (**c**) CF/DF plot for a cylindrical FAIMS device. Traces i, ii, iii, and iv represent the "actual fields" being applied between the electrode walls when CV values of −4.8, −6.0, −3.0, and −10.0 V, respectively, are applied (see text for details).

the cesium ion were acquired at nine different DV values, ranging from 2700 to 5000 V. A sample flow rate of 50 μL/min was used and both the vaporizer and transfer capillary were maintained at room temperature. The optimum CV value of ion transmission was extracted for each DV value and a plot of the CV as a function of the DV for the cesium ion under this set of conditions is shown in Figure 3a.

The following discussion is not meant to be a rigorous treatment of the data but will instead focus on explaining (and predicting) trends observed in the CV spectra. Consequently, effects of diffusion and space-charge repulsion are not included. To describe the fields that an ion experiences within the FAIMS device, the plots can be converted to CF/DF plots, where CF stands

for compensation field and DF stands for dispersion field [17]. Previous work did not include the effect of the gas number density [17]; however, to address the role of temperature, it is necessary to treat the fields as E/N. For illustrative purposes, the conversion of the CV/DV plot to CF/DF will first be considered for a flat-plate FAIMS device (having parallel electrodes, one having the CV/DV applied to it; the other is held at ground potential) and is shown in Figure 3b. In this case, E can be calculated from eq 7 for any given DV value (i.e., Va) for the geometry used in this portion of the study (a = 6.5 mm and b = 9.0 mm as shown in Figure 1). For example, for the data point (labeled as "X" in the figure) having a DV of 3200 V and a CV of −4.8 V, the values of E are 12,800 and −19.2 V/cm, respectively. The value of N can be calculated from eqs 3 and 4 and in this experiment the values of T and p were measured as 309 K and 1.011 atm, respectively. Thus for all points in this experiment, $N = 2.40 \times 10^{19}$ cm^{-3}. Consequently, for DV 3200 V, DF = (12.8 kV cm^{-1})/$(2.40 \times 10^{19}$ cm$^{-3}) = 53.3 \times 10^{-17}$ V/cm$^2 = 53.3$ Td (where 1 "townsend" or "Td" $= 1 \times 10^{-17}$ V/cm^2). Similarly, for CV = −4.8 V, CF = -8.0×10^{-2} Td or −8.0 cTd. All the other data points for the cesium ion in Figure 3b were converted to CF/DF in this manner.

Still considering the flat-plate FAIMS device, because the electric field is uniform between the two electrode walls, only when the correct CV is applied for a given DV value (i.e., must correspond to a point on the line labeled "balance conditions") will the cesium ion be stable between the two electrode walls. Any other applied CV/DV values will cause the cesium ion to drift toward one of the two electrodes, as is indicated in Figure 3b. That is, when CV/DV values are applied that fall below the balance line, the ion will move toward the grounded electrode and when CV/DV values are applied that correspond to a location above the balance line in Figure 3b, the ion will move toward the electrode that has the CV/DV applied to it. Note that the further away from the line that the applied CV/DV value is, the faster the cesium ion will discharge to the walls of the device. Because even small changes in CV from the optimum value will begin to move an ion toward one of the walls, extremely narrow peak widths are possible with enough ion separation time.

The situation for concentric cylinders is different because of the effect of the radial position of the ion on the local voltage and thus the local electric fields. For the cylindrical geometry, the calculation of N is the same as it was for the flat-plate example; however, the calculation of E is now carried out using eq 6. If we assume that the optimal transmission conditions correspond to an ion location near the middle (i.e., r = 7.7 mm) of the gap between the inner and outer electrode, an almost identical balance line is derived as is shown in Figure 3c. However, consider again Point X that corresponds to the optimal transmission of the cesium ion at a CV of −4.8 V when the DV is 3200 V. Because E changes between the two cylinders, it is first useful to

look at the maximum and minimum E/N values that can be derived by looking at ions near the surface of the inner and outer electrodes, respectively. At the surface of the inner electrode (r = 6.5 mm) when the applied DV = 3200 V, E = 1510 V cm^{-1}, and DF = 63.0 Td. Similarly, for CV = −4.8 V, CF = −9.5 cTd. At the surface of the outer electrode, DF = 45.5 Td and CF = −6.8 cTd. These two points are added to the plot in Figure 3c; the dashed line (labeled as trace i) therefore represents the CF and DF values at different radial locations between the two cylindrical electrode walls. The figure shows that when the ion is near the inner electrode, the applied CF is not sufficient to balance the ion between the cylinders for the applied DF and this will cause the ion to move away from the inner electrode and toward the outer electrode (along the dashed line) until it reaches the intersection of the "applied" and "balance" conditions. Conversely when the ion is near the outer electrode, the applied CF is greater than the CF required for balance at the applied DF and this will cause the ion to move away from the outer electrode toward the inner electrode (along the dashed line) until it reaches the intersection of the "applied" and "balance" conditions. Thus, the ion moves away from the cylindrical walls to a location (dictated by the intersection of the applied and balance conditions) between the two electrodes. This atmospheric pressure ion focusing mechanism [17] results in greater signal intensities than what is observed using flat plates, although it also illustrates the restrictions on peak width and peak separation. Consider traces ii–iv in Figure 3c that represent the application of different CV values at a DV of 3200 V. Application of CV = −6.8 V (trace ii) shows that in the majority of the region between the two electrodes that the applied CF is greater than the CF required for balance, thereby moving the ion toward the inner electrode. However, near the inner electrode surface, the plot shows that the applied CF is less than the CF required to balance the ions between the two electrodes. What this means is that at CV = −6.8 V, the ions will be focused toward a region near the inner electrode. Thus, unlike the flat-plate design, an ion can achieve balanced conditions between the electrodes even when the CV is not at the optimum value. By a similar argument, when the CV applied is −3.8 V (trace iii), the focusing region resides near the outer electrode. Trace iv in Figure 3c illustrates that if there is no intersection between the actual and balance conditions then the ion will not transmit through the device. Of course, in the preceding discussion, the consideration is for the *net* motion during one complete cycle of the asymmetric waveform and several cycles may be required for an ion to reach a stable location between the electrode walls. Furthermore, for simplicity in this discussion the consideration of the total distance that the ion moves has been ignored. Note, however, that as this movement becomes significant compared with the distance between the two elec-

trodes, this consideration will play an important role in the signal intensity and peak shape.

Variables Affecting E/N

The preceding discussion provided the basis necessary to look at the effect of variables such as temperature. The effect of temperature was investigated for the cesium ion by using active temperature control of the electrode while acquiring a series of CV plots, each at a fixed temperature. CV spectra for the cesium ion were acquired at nine different DV values ranging from 2700 to 5000 V using a sample flow rate of 50 μL/min. In this experiment, both the vaporizer and transfer capillary were held at room temperature. Figure 4a shows CV/DV plots acquired at electrode temperatures of 36, 55, 75, 95, and 116 °C. As the temperature of the electrodes increases, the magnitude of the optimum CV of transmission also increases because of the effect of temperature on the gas number density, N. Increasing the temperature of the FAIMS electrodes reduces the gas number density, resulting in a higher effective E/N value. For example, calculations using the equations presented earlier illustrate that an increase in the electrode temperature from 36 to 116 °C will significantly increase E/N from 83 to 105 Td when using a DV of 5000 V and a 2.5-mm electrode gap. Consequently, to account for changes in the gas number density, plots were converted to fields and Figure 4b shows the optimal transmission of the cesium ion, plotted as compensation field (CF), versus the dispersion field (DF) for all points shown in Figure 4a. This plot shows that, within experimental error, all the points on the CF/DF plot fall on a single line, illustrating that the changes in CV for the cesium ion are readily accounted for by changes in the gas number density. In other
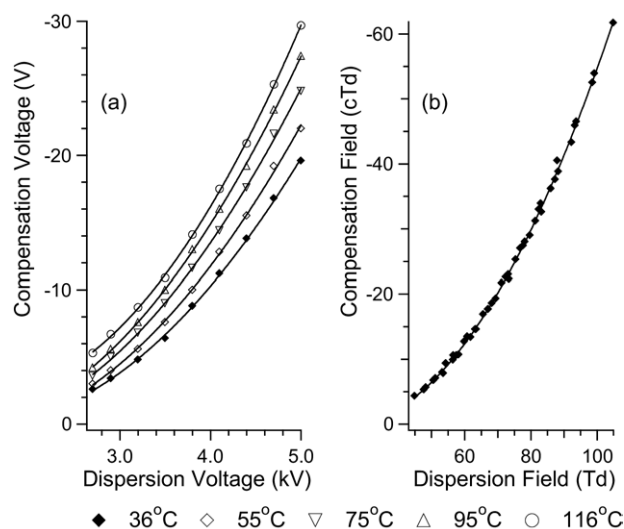

Figure 4. (a) ESI-FAIMS-MS data collected for the cesium cation (*m/z* 133) in nitrogen at electrode temperatures of 36, 55, 75, 95, and 116 °C. (b) Resulting conversion of CV/DV data pairs to field strengths (CF/DF) in units of Townsends.

words, in the absence of any changes in the ion-neutral interactions with temperature, a plot of the compensation field (CF) versus the dispersion field (DF) in Td units is expected to fall on the same line when E/N is varied by temperature. However, as will be subsequently discussed, sometimes when points are obtained at different temperatures, deviations can occur where points do not all fall on the same line and are indicative of changes in ion-neutral interactions that accompany changes in gas number density.

The pressure of the FAIMS system described herein is dependent on ambient atmospheric conditions and elevation. Day-to-day variations in atmospheric pressure in the Ottawa region (where this study was carried out) can be as much as ±20 Torr, or about 5% overall. Figure S2a shows CV/DV data collected for the cesium ion in nitrogen at two different atmospheric pressures, the minimum and maximum pressures observed during the course of this study, 745.9 and 768.8 Torr, respectively. Thus, to account for changes in pressure, the CV/DV plots were converted to CF/DF plots and are shown in Figure S2b. Again, within experimental error, all the points fall on a single line for CF as a function of DF, as would be expected when only the pressure is affecting the gas number density. Unlike temperature, for all the ions investigated in this study, deviations from the single line plot were not observed as a result of changes in pressure.

The preceding discussion has shown that, in the absence of changes in ion-neutral interactions, shifts in the CV can be accounted for through changes in gas number density (i.e., temperature and/or pressure). Another important question is whether changes in CV can be accounted for by changes in the FAIMS geometry (i.e., changing "a" and/or "b" in eq 6). The subtlety in the answer to this question arises because of peak widths. To illustrate this, consider changes in gas number density. For example, if a DV of 5000 V is used and the temperature is 36 °C, E_{flat} = 83.3 Td, E(min) = 71.1 Td, and E(max) = 98.4 Td. If the temperature is increased to 116 °C, the DV can be lowered to 3970 V to give the same E_{flat} value. In addition, the values of E(min) and E(max) remain the same! Consequently, there should be no changes in the determination of the optimal CV value because the spectra obtained using the two different sets of conditions will have the same peak widths. However, consider the situation for the three different FAIMS prototypes that were used in this study; in all cases, b = 9.0 mm and a = 7.0, 6.5, or 6.0 mm. Once again, E_{flat} can be made the same for all prototypes by adjusting the DV to compensate for the change in the gap size between the inner and outer electrodes. The fields near the surfaces of the inner and outer cylindrical electrodes were calculated using eq 6 and the results are shown in Table 1. The results show that the fields near the surfaces of the electrodes are different for each geometry and the implication to the FAIMS data is shown in Figure S3. Figure S3a shows CV plots obtained for protonated lidocaine using the three

Table 1. Effect of changing the inner electrode radius on the electric fields near the electrode walls within the FAIMS device[a]

a (mm)	DV (kV)	E_{min} (Td)	E_{max} (Td)
6.0	6.0	68.5	102.7
6.5	5.0	71.1	98.4
7.0	4.0	73.7	94.7

[a]E_{flat} = 83.3 Td, b = 9.0 mm, T = 36 °C, p = 1.011 atm.

different FAIMS prototypes (same E_{flat} value) and Figure S3b shows the CV plots converted to CF plots. The plots show a dramatic increase in peak width (at 50% maximum intensity) as "a" is decreased. In particular, Figure S3b shows that most of the change in peak width is observed on the high field side of the peak. Consequently, the optimum CV values of transmission for the three prototypes, calculated using the same procedure as shown in Figure S1, are −88.5 cTd (a = 7.0 mm), −93 cTd (a = 6.5 mm), and −101 cTd (a = 6.0 mm). The optimum CV value changes because the capability to prevent ions from colliding with the walls changes with the three prototypes, as was illustrated in Table 1. The main reason that the high field sides of the CV peaks in Figure S3 change more with the prototype than the low field sides is a result of the shape of the CF/DF plots. The CF/DF plot for protonated lidocaine (not shown) has a shape similar to that of the cesium ion shown in Figure 4b; however, the degree of change at high fields is even more pronounced. Consequently, at the higher fields (i.e., near the inner electrode), small changes in E will have more significant effects in terms of the change in CF than will be observed at the lower fields (i.e., near the outer electrode). A similar argument can also be presented to show that the same type of effect can be expected when changing the outer cylinder dimensions while holding the inner cylinder dimensions constant. Note that as the overall dimensions decrease, these effects become more pronounced [25]. Thus, the implications of these results are that, even with correcting for changes in fields, the same optimal values for CF of transmission should not be expected for different geometries.

Deviations Due to Clusters and Ion-Neutral Interactions

The high-field mobility of the iodide anion in a carrier gas of nitrogen increases with increasing electric field strength (i.e., K_h/K > 1) and thus the iodide anion (m/z −127) is an example of an N1-type ion [12]. Application of a negative polarity asymmetric waveform and positive polarity compensation voltage is required for the transmission of the iodide ion through a cylindrical focusing FAIMS device [12]. Figure 5a shows CV/DV data at electrode temperatures of 36 and 116 °C. When converted to field strengths (Figure 5b), this pair of data shows no overlap. Clearly in this case, it is not possible to correct for changes in the CV of transmission for
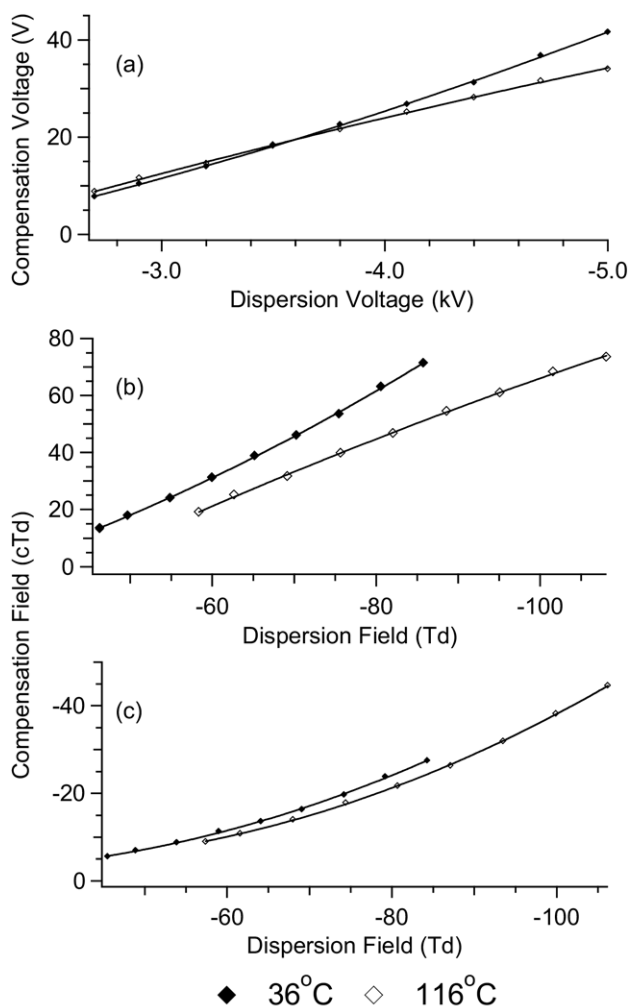
Figure 5. Examples of deviation from expected behavior when comparing data acquired at electrode temperatures of 36 and 116 °C. (**a**) ESI-FAIMS-MS data collected for the iodide anion (*m/z* 127) in nitrogen. (**b**) Conversion of transmission parameters to field strengths (CF/DF) in units of Townsends for iodide in nitrogen. (**c**) CF/DF plots derived from ESI-FAIMS-MS data collected for the $[M+2H]^{2+}$ ion of gramicidin S (*m/z* 571) in a 50/50 mixture of helium/nitrogen.

iodide caused by temperature using only the equations presented earlier. In this example, there is some experimental evidence to support the speculation that the deviation is caused by changes in the formation of clusters between the ions and the bath gas. Ions have been observed to form clusters with the bath gas [22] and this is thought to bring about the conditions for apparent increases in mobility as the field is increased because ions will have a lower effective mass at high-field compared with low-field conditions (i.e., cluster ions contain fewer bath gas molecules). As the temperature is increased, the degree of clustering would also start to decrease at lower field and the effective mass at lower field would eventually begin to approach the effective mass of the cluster (or bare ion) at high field. Experimentally, the change in the shape of the CV/DV plot in Figure 5a would support this explanation. As the

DV is increased (the low-field voltage is half the magnitude of the high-field voltage for the asymmetric waveform used in this study), the combination of increasing the temperature of the bath gas to 116 °C and the additional heating from the electric field (even at low field) starts to reduce the effective mass of the cluster ion. This would begin to result in a reduction in the magnitude of the change of CV with incremental steps of DV, as is observed in the figure. It is expected that at even higher fields, the mass of the cluster would be reduced further, eventually resulting in lower CV values as the DV is incremented further (i.e., the ion would be expected to show type B behavior [26]).

Another interesting example of deviation from predicted behavior involves the $[M+2H]^{2+}$ ion of the peptide gramicidin S. The mobility of the $[M+2H]^{2+}$ ion in a carrier gas of nitrogen decreases with increasing electric field strength and thus doubly protonated gramicidin S (*m/z* 571) is an example of a P2 type ion [12]. Application of a negative polarity asymmetric waveform and negative polarity compensation voltage is required for the transmission of the $[M+2H]^{2+}$ ion of gramicidin S through a cylindrical focusing FAIMS device [12]. CV/DV data at two different temperatures (both electrodes were set at either 36 or 116 °C) were acquired for the $[M+2H]^{2+}$ ion of gramicidin S using a carrier gas of nitrogen (not shown). When these pairs were converted to CF/DF plots, there was an excellent overlap of the datasets. However, for peptide ions, such as the $[M+2H]^{2+}$ ion of gramicidin S, or more generally for P2-type ions, FAIMS analysis is typically carried out in a bath/carrier gas consisting of a 50/50 mixture of nitrogen and helium because this gas mixture generally increases the optimal CV of transmission, separation, and sensitivity for peptide ions [27, 28]. In general, as expected when working at atmospheric pressure, the gas mixture is an extremely important consideration for FAIMS analysis [29]. Collection of the CV/DV data at the two different temperatures was repeated for the $[M+2H]^{2+}$ ion of gramicidin S using the 50/50 helium/nitrogen gas mixture. CF/DF plots obtained from these data (Figure 5c) show a poor overlap, indicating that standardization for temperature effects using only the aforementioned equations is not sufficient. Compared with the example for the iodide anion, the deviation is actually much smaller, suggesting a more subtle change than was observed for the iodide anion. The deviation is very likely caused by changes in ion-neutral interactions that are occurring as a result of elevated temperatures. Various models have been put forth that approximate ion-neutral interactions and have been summarized by Mason and McDaniel [22] and more recently by Eiceman and Karpas [30]. Especially when considering the added complication of ion heating from the applied high fields, a rigorous examination of ion-neutral interactions is beyond the scope of this investigation. In any case, this example illustrates that caution must be taken when comparing datasets obtained at different temperatures because changes to

clusters or ion-neutral interactions can affect the predicted values for CV of ion transmission as given by the equations presented in this document. Analytically, for good method reproducibility, the temperature needs to be maintained at a fixed value, a condition that is readily implemented with the temperature controlled electrode set.

Resolution and Temperature Differentials

The mobility of the $[M-H]^-$ ion of taurocholic acid in a carrier gas of nitrogen decreases with increasing electric field strength. Deprotonated taurocholic acid (m/z -514) is therefore an example of an N2-type ion. Application of a positive polarity asymmetric waveform and positive polarity compensation voltage is required for the transmission of the $[M-H]^-$ ion of taurocholic acid through a cylindrical focusing FAIMS device [12]. Deprotonated taurocholic acid or type N2 ions are also typically analyzed by FAIMS in a bath/carrier gas consisting of a 50/50 mixture of nitrogen and helium. Conversion of CV/DV data to CF/DF data (the latter is shown in Figure 6) collected in a helium/nitrogen gas mixture results in the data overlapping on the same line, indicating that the aforementioned equations can be used to describe changes in temperature
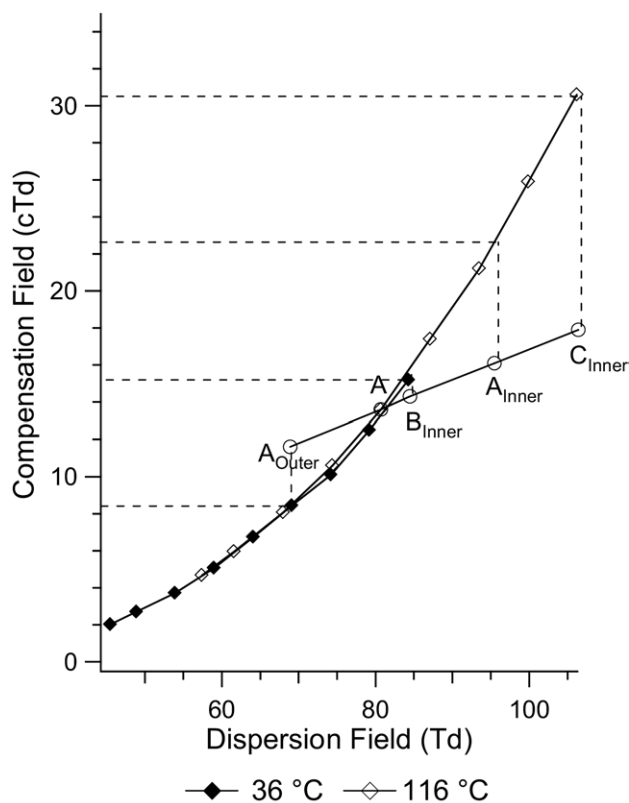

Figure 6. CF/DF plots derived for ESI-FAIMS-MS data collected for the $[M-H]^-$ ion of taurocholic acid (m/z 514) in a gas mixture of 50/50 helium/nitrogen at electrode temperatures of 36 and 116 °C. The effect of changing the inner electrode temperature is illustrated using the plot (see text for details).

and that changes in the ion-neutral interactions are not significant over this temperature range. This plot will be used to illustrate how temperature can be used to improve the resolution between two ions that are close together in CV.

Figure S4 shows ion-selected compensation voltage (IS-CV) plots collected for the pseudo-molecular $[M-H]^-$ ions of taurocholic acid (m/z -514) and methotrexate (m/z -453) at electrode temperatures of 36, 76, and 116 °C in 50/50 helium/nitrogen. As the temperature increases, the width of the IS-CV peaks increases and the overlap between the two species increases. Resolution, defined by the following equation, can be used to quantify the separation of the two compounds:

$$R_s = 2 * (CV_1 - CV_2)/(PW_1 + PW_2) \qquad (8)$$

where CV_1 and CV_2 are the compensation voltage values observed for the two species and PW_1 and PW_2 are the peak widths at 10% height for the two species. In general, as the value of R_s increases, the resolution of two analyte ions improves.

A feature of using separate heated gas supplies to control the temperature of the electrodes is that the temperature of the two electrodes can be varied independently. Individual control of the electrode temperatures offers extra flexibility to control the compensation voltage, peak width, separation, and sensitivity for different analytes. In some cases, baseline separation of two components is required when the presence of one component can affect the analysis of the other [9]. Conversely, for analyzing a compound using an internal standard, it is desirable to have both species transmit at the same CV value. The effect of using differential temperatures on the separation of taurocholic acid and methotrexate is shown in Figure 7. In all cases in the figure, the outer electrode temperature was kept constant at 76 °C, whereas the inner electrode temperature was set to 36 °C (Figure 7a), 76 °C (Figure 7b), and 116 °C (Figure 7c). Through the use of a lower inner electrode temperature, it is possible to achieve baseline resolution of the two components as shown in Figure 7a ($R_s = 1.51$) or, with the use of a higher inner electrode temperature, significant overlap of the two components as shown in Figure 7c ($R_s = 0.15$) can be obtained.

How the changing temperature differentials affect the peak width, and thus the resolution, is illustrated using Figure 6. The situation has similarities to what was described for the cesium ion in Figure 3. Because we have determined that changes in ion-neutral interactions are not significant between 36 and 116 °C, the CV/DV value for any temperature between these two points can be interpolated from the line. By taking point A from the plot in Figure 6, we can use the equations to determine that at 76 °C, the DV is 4235 V and the CV is 7.15 V. Using these values, the fields at the surfaces of the inner and outer electrodes can be determined. For the outer electrode, the DF = 68.9 Td and CF = 11.6 cTd, whereas for the inner electrode, DF = 95.5 Td and
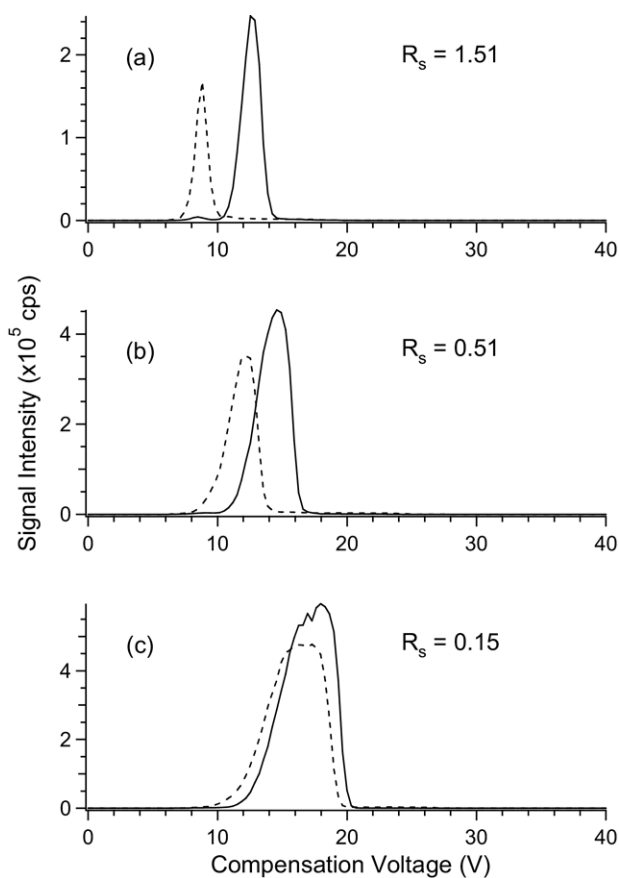
Figure 7. Resolution of the [M−H]⁻ ions of taurocholic acid (*m/z* 514) and methotrexate (*m/z* 453) using differential electrode temperatures of (T_{inner}/T_{outer}): (**a**) 36 °C/76 °C, (**b**) 76 °C/76 °C, and (**c**) 116 °C/76 °C. The DV was 5.0 kV and p = 0.999 atm.

CF = 16.1 Td. A solid line has been added to the plot to illustrate the actual fields between the two electrode walls, A_{Inner} and A_{Outer}. By changing the CV value, this line will effectively shift upward or downward on the plot as was illustrated in Figure 3c. As a crude first approximation for the peak width, the values where A_{Inner} and A_{Outer} intersect the balance line can be used. As is illustrated by the dashed line in the figure, these values correspond to about 8.5 cTd (A_{Outer}) and 22.6 cTd (A_{Inner}). At 76 °C, this corresponds to CV values of 5.2 and 10.0 V. Thus, the approximate CV of transmission would be 7.6 V and the baseline peak width would be approximately 4.8 V. When the inner electrode temperature is lowered to 36 °C, the field near the outer surface will remain unchanged; however, the applied fields near the inner electrode will decrease due to the change in temperature. Calculation of the fields give a DF = 84.5 Td and CF = 14.3 cTd and is shown by B_{Inner}, which has been added to the plot in the figure. In this instance, B_{Inner} will intersect the balance line at 15.4 cTd, which at 36 °C corresponds to a CV value of 7.7 V. Consequently, by decreasing the inner electrode temperature, the approximate CV of transmission would now be lowered to 6.5 V and the baseline peak width would decrease to about 2.5 V. Conversely, increasing

the inner electrode temperature will increase the magnitude of the fields near the inner electrode. That is, when the inner electrode temperature is raised to 116 °C, DF = 106.4 Td and CF = 17.9 cTd, as is illustrated by C_{Inner}, which has been added to the plot in Figure 6. C_{Inner} will intersect the balance line at 30.5 cTd, which at 116 °C corresponds to a CV value of 12.1 V. Thus, by increasing the inner electrode temperature, the approximate CV of transmission would now be increased to 8.7 V and the baseline peak width has increased to about 6.9 V. In addition, the change in signal intensity is also consistent with the plots in Figure 6. The difference between the actual and balanced fields near the electrode walls gives an indication of the magnitude of the focusing field. Because this difference is smallest with the lowest inner electrode temperature (i.e., weakest focusing field), to a first approximation, it is expected that this situation will suffer the most ion losses due to diffusion and space-charge repulsion resulting in the lowest signal intensity.

The preceding explanation is consistent with the data shown in Figure 7. That is, for the [M−H]⁻ ion of taurocholic acid, when the temperature of the inner electrode is elevated relative to the temperature of the outer electrode, the CV of optimal transmission will shift to larger values and wider peaks (and greater signal intensities) are to be expected. Conversely, when the temperature of the inner electrode is lowered relative to the temperature of the outer electrode, the CV of optimal transmission will shift to smaller values and narrower peaks (and lower signal intensities) are to be expected. All ions with similar CF/DF plots would be expected to behave in an analogous fashion (assuming they do not experience changes in ion-neutral interactions), although generalizations for all ions must not be inferred from this example. The shape of the CF/DF plot is obviously critical in determining the effect of temperature and radically different behavior can be envisioned, for example, for a B-type ion [26]. Nonetheless, these examples illustrate the power in using the independent temperature control to adjust separation capability.

Conclusions

A FAIMS device that uses high flow rate, temperature-controlled gases passing through channels drilled into the FAIMS electrodes has been developed to control the temperature of the FAIMS electrode set independent from other external heat sources in the atmospheric pressure interface, such as the ionization source. Active heating (or cooling) of the electrodes allows rapid stabilization of the FAIMS transmission conditions (i.e., CV), improving the reliability and ruggedness of the device, and gives more flexibility when compared with previous designs. The effect of pressure and electrode temperature on ion transmission and separation through FAIMS is described using fields and CF/DF plots. For some ions, such as cesium or taurocholic acid,

these plots are sufficient to fully explain changes caused by the effect of temperature (and pressure) in the gas number density. However, for other ions, deviations from predicted behavior are observed. Experimental evidence suggests these deviations are caused by changes in the degree of cluster formation (e.g., iodide anion in nitrogen) or by changes in ion-neutral interactions (e.g., $[M+2H]^{2+}$ ion of gramicidin S in a nitrogen/helium bath gas) that could not be predicted using the equations presented herein.

From a practical standpoint, for day-to-day operations, changes in the CV of ion transmission caused by pressure effects are shown to be predictable and can be readily accounted for, which is an important consideration for comparisons of work done at different geographical locations. However, comparisons of data obtained at different electrode temperatures can be misleading (i.e., if the ion deviates from predicted behavior) and, ideally, data comparisons should be made at the same electrode temperatures (readily achievable with temperature control). Separately controlling the temperature on the inner and outer electrodes is shown to be an extremely useful parameter for manipulating the selectivity of FAIMS. Previous designs were restricted by the temperature dictated by indirect heating of the FAIMS electrodes (and therefore had no flexibility), whereas the current design can be used either to increase separation between species (e.g., analyte and interferent peaks) or to increase overlap between species (e.g., analyte and internal standard peaks) by adjusting settings for electrode temperature. Because optimal temperature settings depend on the shape of the CF/DF plots, optimal temperature settings will vary and therefore need to be determined experimentally.

References

1. Wilson, I. D.; Plumb, R.; Granger, J.; Major, H.; Williams, R.; Lenz, E. M. HPLC-MS-based Methods for the Study of Metabonomics. *J. Chromatogr. B* **2005**, *817*, 67–76.
2. Want, E. J.; Nordstrom, A.; Morita, H.; Siudzak, G. From Exogenous to Endogenous: The Inevitable Imprint of Mass Spectrometry in Metabolomics. *J. Proteome Res.* **2007**, *6*, 459–468.
3. Hughes, N.; Winnik, W.; Dunyach, J.; Amad, M.; Splendore, M.; Paul, G. High-Sensitivity Quantitation of Cabergoline and Pergolide Using a Triple-Quadrupole Mass Spectrometer with Enhanced Mass-Resolution Capabilities. *J. Mass Spectrom.* **2003**, *38*, 743–751.
4. Yamashita, M.; Fenn, J. B. Electrospray Ion Source. Another Variation on the Free-Jet Theme. *J. Phys. Chem.* **1984**, *88*, 4451–4459.
5. Fenn, J. B.; Mann, M.; Meng, C. K.; Wong, S. F.; Whitehouse, C. M. Electrospray Ionization for Mass Spectrometry of Large Biomolecules. *Science* **1989**, *246*, 64–71.
6. Bruins, A. P.; Covey, T. R.; Henion, J. D. Ion Spray Interface for Combined Liquid Chromatography/Atmospheric Pressure Ionization Mass Spectrometry. *Anal. Chem.* **1987**, *59*, 2642–2646.
7. Covey, T.; Henion, J. Direct Liquid Introduction/Thermospray Interface for Liquid Chromatography/Mass Spectrometry. *Anal. Chem.* **1983**, *55*, 2275–2280.
8. Mahan, E. A.; King, R. The Use of LC-APCI-FAIMS-MS for the Quantitative Analysis of Taxol in Mouse Plasma. Proceedings of the 53rd ASMS Conference on Mass Spectrometry and Allied Topics, San Antonio, TX; June 5–9, 2005.
9. Kapron, J. T.; Jemal, M.; Duncan, G.; Kolakowski, B.; Purves, R. W. Removal of Metabolite Interference during Liquid Chromatography/Tandem Mass Spectrometry Using High-Field Asymmetric Waveform Ion Mobility Spectrometry. *Rapid Commun. Mass Spectrom.* **2005**, *19*, 1–6.
10. Buryakov, I. A.; Krylov, E. V.; Nazarov, E. G.; Rasulev, U. K. A New Method of Separation of Multi-atomic Ions by Mobility at Atmospheric Pressure Using a High-Frequency Amplitude-Asymmetric Strong Electric Field. *Int. J. Mass Spectrom. Ion. Process.* **1993**, *128*, 143–148.
11. Purves, R. W.; Guevremont, R.; Day, S.; Pipich, C. W.; Matyjaszczyk, M. S. Mass Spectrometric Characterization of a High-Field Asymmetric Waveform Ion Mobility Spectrometer. *Rev. Sci. Instrum.* **1998**, *69*, 4094–4105.
12. Purves, R. W.; Guevremont, R. Electrospray Ionization-High Field Asymmetric Waveform Ion Mobility Spectrometry-Mass Spectrometry. *Anal. Chem.* **1999**, *71*, 2346–2357.
13. Guevremont, R.; Ding, L.; Ells, B.; Barnett, D. A.; Purves, R. W. Atmospheric Pressure Ion Trapping in a Tandem FAIMS-FAIMS Coupled to a TOFMS: Studies with Electrospray Generated Gramicidin S Ions. *J. Am. Soc. Mass Spectrom.* **2001**, *12*, 1320–1330.
14. Levin, D. S.; Miller, R. A.; Nazarov, E. G.; Vouros, P. Rapid Separation and Quantitative Analysis of Peptides Using a New Nanoelectrospray-Differential Mobility Spectrometer-Mass Spectrometer System. *Anal. Chem.* **2006**, *78*, 5443–5452.
15. Tang, K.; Li, F.; Shvartsburg, A. A.; Strittmatter, E. F.; Smith, R. D. Two-Dimensional Gas-Phase Separations Coupled to Mass Spectrometry for Analysis of Complex Mixtures. *Anal. Chem.* **2005**, *77*, 6381–6388.
16. Shvartsburg, A. A.; Li, F.; Tang, K.; Smith, R. D. High-Resolution Field Asymmetric Waveform Ion Mobility Spectrometry Using New Planar Geometry Analyzers. *Anal. Chem.* **2006**, *78*, 3706–3714.
17. Guevremont, R.; Purves, R. W. Atmospheric Pressure Ion Focusing in a High-Field Asymmetric Waveform Ion Mobility Spectrometer. *Rev. Sci. Instrum.* **1999**, *70*, 1370–1383.
18. Ells, B.; Barnett, D. A.; Purves, R. W.; Guevremont, R. Detection of Nine Chlorinated and Brominated Haloacetic Acids at Part-per-trillion Levels Using ESI-FAIMS-MS. *Anal. Chem.* **2000**, *72*, 4555–4559.
19. Li, J.; Purves, R. W.; Richards, J. C. Coupling Capillary Electrophoresis and High-Field Asymmetric Waveform Ion Mobility Spectrometry Mass Spectrometry for the Analysis of Complex Liposaccharides. *Anal. Chem.* **2004**, *76*, 4676–4683.
20. Kapron, J. T.; Wu, J.; Mauriala, T.; Clark, P.; Purves, R. W.; Bateman, K. Simultaneous Analysis of Prostanoids Using Liquid Chromatography/High-Field Asymmetric Waveform Ion Mobility Spectrometry/Tandem Mass Spectrometry (LC-FAIMS-MS/MS). *Rapid Commun. Mass Spectrom.* **2006**, *20*, 1–8.
21. Barnett, D. A.; Guevremont, R.; Purves, R. W. Design and Characterization of a Temperature Controlled FAIMS System for Small Molecule Analysis. Proceedings of the 53rd ASMS Conference on Mass Spectrometry and Allied Topics, San Antonio, TX; June 5–9, 2005.
22. Mason, E. A.; McDaniel, E. W. Transport Properties of Ions in Gases. New York: Wiley; **1988**, 389–398.
23. Viehland, L. A.; Guevremont, R.; Purves, R. W.; Barnett, D. A. Comparison of High-Field Ion Mobility Obtained from Drift Tubes and a FAIMS Apparatus. *Int. J. Mass Spectrom.* **2000**, *197*, 123–130.
24. Guevremont, R.; Barnett, D. A.; Purves, R. W.; Viehland, L. A. Calculation of Ion Mobilities from Electrospray Ionization High-Field Asymmetric Waveform Ion Mobility Mass Spectrometry Data. *J. Chem. Phys.* **2001**, *114*, 10270–10277.
25. Guevremont, R.; Purves, R. W. Comparison of Experimental and Calculated Peak Shapes for Three Cylindrical Geometry FAIMS Prototypes of Differing Electrode Diameters. *J. Am. Soc. Mass Spectrom.* **2005**, *16*, 349–362.
26. Shvartsburg, A. A.; Bryskiewicz, T.; Purves, R. W.; Tang, K.; Guevremont, R.; Smith, R. D. Field Asymmetric Waveform Ion Mobility Spectrometry Studies of Proteins: Dipole Alignment in Ion Mobility Spectrometry. *J. Phys. Chem. B* **2006**, *110*, 21966–21980.
27. McCooeye, M. A.; Ells, B.; Barnett, D. A.; Purves, R. W.; Guevremont, R. Quantitation of Morphine and Codeine in Human Urine Using High-Field Asymmetric Waveform Ion Mobility Spectrometry (FAIMS) with Mass Spectrometric Detection. *J. Anal. Toxicol.* **2001**, *25*, 81–87.
28. Barnett, D. A.; Ells, B.; Guevremont, R.; Purves, R. W. Application of ESI-FAIMS-MS to the Analysis of Tryptic Peptides. *J. Am. Soc. Mass Spectrom.* **2002**, *13*, 1282–1291.
29. Shvartsburg, A.; Tang, K.; Smith, R. D. Understanding and Designing Field Asymmetric Waveform Ion Mobility Separations in Gas Mixtures. *Anal. Chem.* **2004**, *76*, 7366–7374.
30. Eiceman, G. A.; Karpas, Z. Ion Mobility Spectrometry, 2nd ed. New York: Taylor & Francis; 2005.